Biomaterials Science

ROYAL SOCIETY OF CHEMISTRY

PAPER

View Article Online
View Journal | View Issue

Check for updates

Cite this: *Biomater. Sci.*, 2020, **8**, 2007

Enzyme-instructed assembly of a cholesterol conjugate promotes pro-inflammatory macrophages and induces apoptosis of cancer cells†

Yuan Hu,[a,b] Huaimin Wang,[c] Chenge Li,[a,b,d] Jinyao Liu, *[a,b,d] Bing Xu *[c] and Wen Di*[a,b,e]

The combination of immunotherapy and chemotherapy has shown great potential for treating solid tumors. Although various combination therapy regimens have been demonstrated to be effective, their implementation in practice always needs separate drugs or modalities, which in turn requires specific and complicated operation procedures. Here, we describe the use of enzyme-instructed self-assembly (EISA) of a phosphotyrosine–cholesterol (PTC) conjugate to combine immune microenvironment modulation and chemotherapy. The enzymatic dephosphorylation of PTC results in the assembly of its derivatives inside and outside the cells, which leads to repolarization of the macrophage phenotype and direct death of cancer cells. The generation of reactive oxygen species and actin disturbance induced by the assemblies has been verified relative to the macrophage repolarization. We also demonstrate its dual repolarization and inhibition effects *in vivo* using an ovarian cancer bearing immunocompetent murine model. The EISA of cholesterol conjugates is an effective yet simple approach for the combination of tumor microenvironment immunomodulation and chemotherapy.

Received 21st January 2020,
Accepted 11th February 2020

DOI: 10.1039/d0bm00125b

rsc.li/biomaterials-science

Published on 12 February 2020. Downloaded by Westlake University on 6/12/2025 7:47:11 AM.

Introduction

The treatment of cancer has undergone evolutionary changes as advances in new technologies are taking place every day and the understanding of the underlying biological processes is increasing.[1–4] Combination therapy, in particular, the combination of immunotherapy and chemotherapy, has shown great potential for treating various cancers with a few clinical trials underway.[5–8] Intensive research on cancer immunotherapy has provided growing evidence that clinical response to chemotherapy can be improved when immune cells are activated or immune suppression is relieved.[9,10] Although a variety of chemoimmunotherapy regimens have been successful in improving treatment efficacy, their transformation into practice inevitably needs more than one therapeutic agent or modality, which in turn requires specific and sophisticated operation procedures. These limitations thus highlight the need for an effective yet simple approach toward chemoimmunotherapy that can be accomplished by using either a single therapeutic agent or a facile process.[11,12]

Enzyme-instructed self-assembly (EISA), a ubiquitous process existing in nature, plays numerous roles and underlines the formation of a wide range of biological complexes.[13,14] EISA is a process that starts from the assembly of small-molecular precursors that undergo enzymatic reactions to initiate the supramolecular self-assembly of their derivatives *in situ* either on the surface or inside of cells.[15] In virtue of its ability to interact with proteins, enzymes and others, EISA is a unique molecular approach to modulate cellular functions and behaviors, exhibiting a wide range of biomedical applications in cancer therapy, molecular imaging and tissue engineering.[16–21] In our previous study, phosphorylated cholesterol conjugates have been demonstrated to self-assemble into nanoparticles *in situ* by enzymatic dephosphorylation, which can effectively and selectively inhibit the growth of many different types of cancer cells,[22] as well as minimize

[a]*Department of Obstetrics and Gynecology, Ren Ji Hospital, School of Medicine, Shanghai Jiao Tong University, Shanghai 200127, China. E-mail: diwen163@163.com, jyliu@sjtu.edu.cn*
[b]*Shanghai Key Laboratory of Gynecologic Oncology, Ren Ji Hospital, School of Medicine, Shanghai Jiao Tong University, Shanghai 200127, China*
[c]*Department of Chemistry, Brandeis University, Waltham, Massachusetts 02453, USA. E-mail: bxu@brandeis.edu*
[d]*Institute of Molecular Medicine, Ren Ji Hospital, School of Medicine, Shanghai Jiao Tong University, Shanghai 200240, China*
[e]*State Key Laboratory of Oncogenes and Related Genes, Shanghai Cancer Institute, Ren Ji Hospital, School of Medicine, Shanghai Jiao Tong University, Shanghai 200127, China*

†Electronic supplementary information (ESI) available. See DOI: 10.1039/d0bm00125b

Published on 12 February 2020. Downloaded by Westlake University on 6/12/2025 7:47:11 AM.

the evolution of acquired drug resistance.[23] As a key component of lipid rafts, cholesterol and its derivatives have proven their capability to potentiate the antitumor response of immune cells, for example, improving the effector function and enhancing the proliferation of CD8+ T cells by modulating cholesterol metabolism.[24,25] In view of these characteristics, the EISA of phosphorylated cholesterol conjugates may have an effect on immune microenvironment modulation in addition to its direct inhibition of cancer cell proliferation, and may be an alternative for chemoimmunotherapy.

Tumor-associated macrophages (TAMs), representing the largest component in the tumor microenvironment, govern tumor progression by either facilitating tumor growth *via* inducing angiogenesis, invasion and immunosuppression, or establishing antitumor immunity by engulfing and killing cancer cells. These dual roles are ascribed to the phenotypic polarity of TAMs, which are typically classified as pro-inflammatory M1 and immunosuppressive M2 macrophages.[26,27] Given their phenotypic and functional plasticity, TAMs have been recognized as potential regulatory targets for combination cancer therapy.[28–30] Here, we describe the use of EISA of a phosphotyrosine–cholesterol (PTC) conjugate to combine immune microenvironment modulation and chemotherapy (Fig. 1). The enzymatic dephosphorylation of PTC results in the assembly of its derivative, which simultaneously promotes pro-inflammatory macrophage polarization and induces direct death of cancer cells. Upon exposure to PTC, a variety of M2 macrophages derived from ovarian cancer patients' ascites, human monocytes and mice display increased mRNA expression associated with pro-inflammatory M1-like responses. The generation of reactive oxygen species (ROS) and actin disturbance induced by the assemblies is confirmed relative to the macrophage repolarization. Meanwhile, the EISA of PTC shows a potent inhibitory effect against both human SKOV3 and murine ID8 ovarian cancer cells. We also demonstrate the dual repolarization and inhibition effects *in vivo* by showing an increased number of pro-inflammatory M1 macrophages in tumor tissues and significantly inhibited tumor growth in an immunocompetent murine model of ovarian cancer. The EISA of cholesterol conjugates opens a new window for combination cancer therapy.

Materials and methods

Cell culture and treatment

The human epithelial ovarian cancer cell line SKOV3, human monocyte cell line THP-1 and mouse macrophage cell line RAW264.7 were obtained from the Cell Bank of the Chinese Academy of Sciences (Shanghai, China). The mouse ovarian cancer cell line ID8 was a kind gift from Dr Katherine F. Roby (University of Kansas Medical Center, Kansas, USA). SKOV3, THP-1 and ID8 were cultured in RPMI-1640 medium (Hyclone, UT, USA), RAW264.7 was cultured in DMEM/F12 medium (Hyclone, UT, USA), all supplemented with 10% fetal bovine serum (FBS) (Gibco, CA, USA) and penicillin/streptomycin (1 : 100, Sigma-Aldrich, MO, USA) in a humid atmosphere incubator with 5% CO_2 at 37 °C. To induce differentiation into the

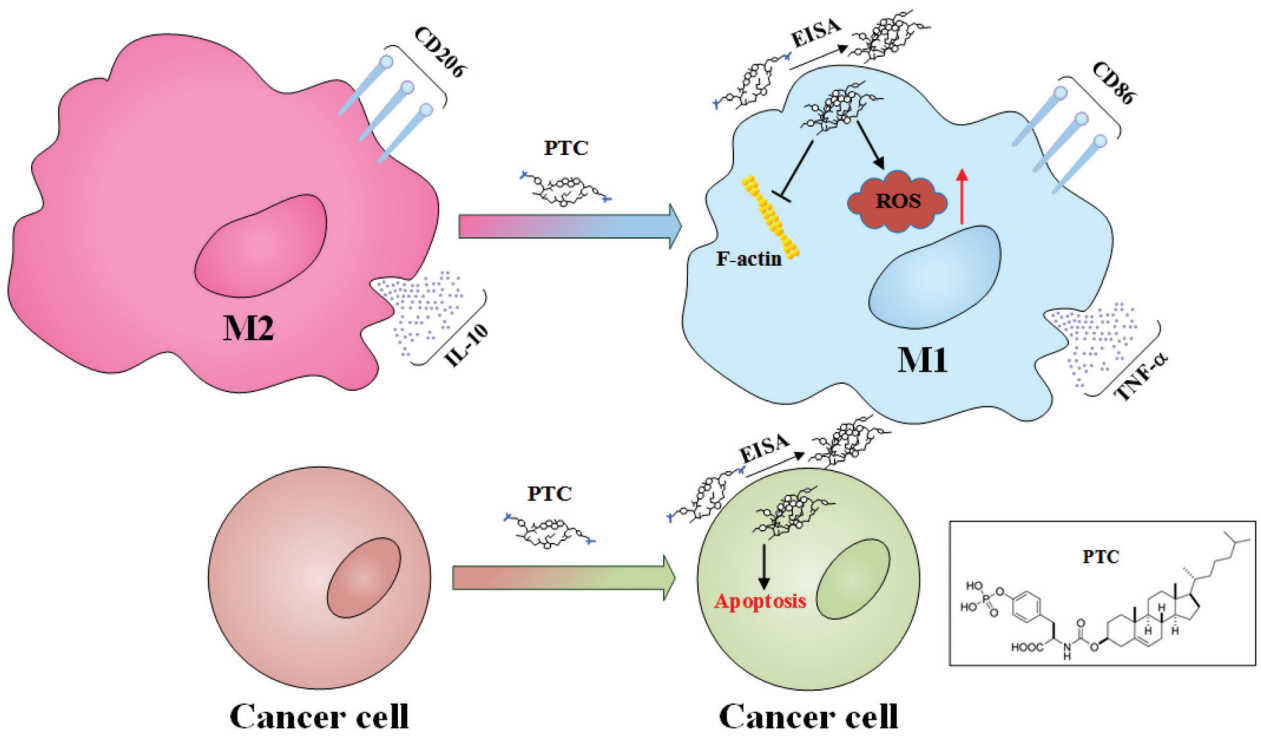

Fig. 1 Enzyme-instructed supramolecular assembly of PTC promotes pro-inflammatory macrophages and induces apoptosis of cancer cells.

 This journal is © The Royal Society of Chemistry 2020

Published on 12 February 2020. Downloaded by Westlake University on 6/12/2025 7:47:11 AM.

macrophages, THP-1 cells (5×10^5 mL^{-1}) were treated with 100 ng mL^{-1} phorbol 12-myristate 13-acetate (PMA) (Sigma-Aldrich) and incubated for 48 h in the complete medium to generate THP-1 macrophages (M0). To obtain M2-polarized THP-1 macrophages, M0 were then cultured with 20 ng mL^{-1} IL-4 and 20 ng mL^{-1} IL-13 for another 48 h. To obtain M2-polarized RAW264.7 macrophages, 5×10^5 mL^{-1} RAW264.7 cells were treated with 20 ng mL^{-1} IL-4 for 24 h. M2 macrophages were treated with PTC for 48 h. PTC was synthesized according to the previously reported protocol.[22]

Quantitative real-time polymerase chain reaction (qRT-PCR) analysis

The total RNA obtained from the macrophages was extracted using the Trizol reagent (Invitrogen, CA, USA). The PrimeScript™ RT Reagent Kit (Cat. RR037A) and SYBR Premix Ex Taq™ (Cat. RR420A) (Takara Bio, DaLian, China) were used to reverse transcribe and perform quantitative PCR of mRNAs according to the manufacturer's protocol. The sequences of human IL-10 are as follows: forward: CACTGCTCTGTTGCCTGGTC, REVERSE: GAAGCATGTTAGGCAGGTTGC. The sequences of human CD206 are as follows: forward: CCGTATGCCGGTCACTGTTA, reverse: CAATTCCTCGATGGTGTGGA. The sequences of human TNFα are as follows: forward: TGGCGTGGAGCTGAGAGATA, reverse: GGAGGTTGACCTTGGTCTGG. The sequences of human iNOS are as follows: forward: TCCAGCCGTGCCACCATCC, reverse: CCACCACTCGCTCCAGGATACC. The sequences of murine IL-10 are as follows: forward: TCCTTACTGCAGGACTTTAAGG, reverse: TATTCTCACAGGGGAGAAATCG. The sequences of murine CD206 are as follows: forward: CCTATGAAAATTGGGCTTACGG, reverse: CTGACAAATCCAGTTGTTGAGG. The sequences of murine TNFα are as follows: forward: ATGTCTCAGCCTCTTCTCATTC, reverse: GCTTGTCACTCGAATTTTGAGA. The sequences of murine iNOS are as follows: forward: GTTTACCATGAGGCTGAAATCC, reverse: CCTCTTGTCTTTGACCCAGTAG. GAPDH was used for data normalization of the mRNA expression. The data were calculated using the $2-\Delta\Delta CT$ method.

Enzyme-linked immunosorbent assay (ELISA)

To evaluate the secretion cytokines of both THP-1 derived and RAW264.7 derived M2 macrophages after PTC treatment, 2 mL supernatants were collected after PTC treatment for 48 h. IL-10 and TNF-α levels were determined by human or mouse ELISA kits (R&D, MN, USA) according to the manufacturer's instructions.

Isolation of macrophages from ovarian cancer patients' ascites

Ascites were obtained from six ovarian cancer patients during their tumor debulking operation at Renji Hospital, School of Medicine, Shanghai Jiao Tong University. The study was approved by the Institutional Review Board of Renji Hospital, School of Medicine, Shanghai Jiao Tong University. Written informed consent was obtained from the patients. Freshly obtained ascites were mixed with heparin and then centrifuged at 1500 rpm for 10 min at room temperature. The upper part was removed, and the residue was precipitated and the precipitate was washed and resuspended with the same volume of PBS. The mononuclear cells were obtained by Ficoll-Paque (GE Healthcare Life Sciences) density centrifugation. The obtained cells were resuspended in RPMI-1640 medium with 10% FBS and penicillin/streptomycin in a humid atmosphere incubator with 5% CO_2 at 37 °C overnight. After the removal of the supernatant the next day, the cells were treated with 5 μg mL^{-1} of PTC and then collected for macrophage identification following 48 h incubation by flow cytometric analysis.

Flow cytometric analysis

Macrophages derived from THP-1 monocytes and ovarian cancer patients' ascites were collected and incubated with anti-human CD68-FITC, CD206-PE and CD86-APC (BD Pharmingen, USA). Both CD68 and CD206 positive cells were regarded as M2 macrophages, while both CD68 and CD86 positive cells were considered as M1 macrophages. Macrophages derived from RAW264.7 and cells isolated from subcutaneous tumors of C57BL/6 were incubated with anti-mouse PE-F4/80, PE-Cy7-CD86 (BD Pharmingen, USA), and anti-mouse PerCP/Cy5.5-CD206 (Biolegend, CA, USA). Both F4/80 and CD206 positive cells were deemed as M2 macrophages, while both F4/80 and CD86 positive cells were considered as M1 macrophages. Samples were handled following the manufacturer's instructions and analyzed by flow cytometry (Beckman FC500 MPL, USA).

ROS assay

Macrophages were seeded in 6-well plates at a density of 5×10^5 cells per mL and treated with PTC for 48 h. After removing the culture media, the cells were rinsed with PBS and then mixed with 1 mL per dish of the probe solution (10 μmol l^{-1}) from the ROS Assay Kit (Beyotime, Shanghai, China). Following 20 min incubation at 37 °C, the cells were washed with PBS and then separately analyzed using a Nikon eclipse TE300 microscope (Tokyo, Japan) and a microplate reader (Thermo Varioskan Flash, USA) and by flow cytometry. The excitation and emission wavelengths were set at 488 nm and 525 nm, respectively.

Actin staining

Macrophages were seeded in 6-well plates at a density of 5×10^5 cells per mL, and treated with PTC for 48 h. After removing the culture media, the cells were gently washed once with PBS and then fixed with 4% paraformaldehyde. Afterward, 200 μl of 100 nM rhodamine phalloidin (Cytoskeleton, CO, USA) was added in the dark and further cultured for 30 min at room temperature. The cells were rinsed with PBS and stained with DAPI (Beyotime, Shanghai, China) for 10 min. Images were obtained using a microscope.

Cell viability assay

To evaluate the cell viability after PTC treatment, we used two methods: CCK-8 assay and apoptosis experiment. For the CCK-8 assay, SKOV3, ID-8, THP-1 derived macrophages and

Published on 12 February 2020. Downloaded by Westlake University on 6/12/2025 7:47:11 AM.

RAW264.7 derived macrophages were separately seeded in 96-well plates and treated with PTC at concentrations of 0, 0.05, 0.1, 0.5, 1, 5, 10, 50, and 100 μg mL^{-1} for 48 h. The absorbance was determined at the wavelength of 450 nm using a microplate reader.

Apoptosis assay

The Annexin V-FITC/propidium iodide (PI) apoptosis detection kit (BD, USA) was used to detect the rate of cell apoptosis. After exposure to PTC, SKOV3 and ID8 cells were treated according to the protocol and analyzed by flow cytometry.

In vivo antitumor activity

5-Week-old female C57BL/6 mice were purchased from Shanghai Jiao Tong University School of Medicine (Shanghai, China) and maintained under SPF conditions. All the animal experiments were performed according to the Shanghai Medical Experimental Animal Care Guidelines. The animal protocols were approved by the Institutional Animal Care and Use Committee of Shanghai Jiao Tong University School of Medicine. ID8 cells (4.5×10^6) were injected subcutaneously at a volume of 100 μl into the bilateral flank of mice. 28 days after tumor cell implantation, the mice were divided randomly into two groups (five animals per group) and intratumorally injected with PBS or 5 mg kg^{-1} of PTC every two days. Tumor tissues were harvested after 6 injections. Tumor growth and mouse body weights were also observed and recorded during the injections. A Vernier caliper was used to estimate the tumor size and the tumor volume was calculated according to the following equation: $V = D_{max} \times D^2_{min}/2$. D_{max} and D_{min} represent the maximum and minimum diameters, respectively.

Immunohistochemical (IHC) staining, immunofluorescence (IF) and hematoxylin and eosin (H&E) staining

C57BL/6 tumor tissues were fixed, embedded in paraffin and sectioned into 4 μm thick sections. After deparaffinization and rehydration, the sections were blocked and then incubated with cleaved caspase-3 (Asp175) (5A1E) rabbit mAb #9664 (Cell Signaling Technology, USA) for IHC staining, anti-mouse CD206 and CD86 (Abcam, Cambridge, UK) for IF. Images were scanned at 40× magnification using a Pannoramic MIDI (3D HISTECH, Budapest, Hungary). IHC scoring was based on the intensity and extent of staining and was evaluated according to the following histological scoring method: 0, negative staining; 1, weak staining; 2, moderate staining; 3, strong staining. The mean proportion of staining cells per specimen was determined semi-quantitatively and scored as follows: 0 for staining <1%, 1 for 1–25%, 2 for 26–50%, 3 for 51–75%, and 4 for >75% of the examined cells. The histological score (H-score) for each specimen was computed using the formula: H-score = proportion score × intensity score. Tissues from the heart, liver, spleen, kidneys and lungs were stained with H&E. Images were obtained using a microscope.

Statistical analyses

All statistical analyses in this study were performed using Prism 5.0 software (GraphPad, Inc, San Diego, CA, USA). Data are presented as means ± standard deviation (SD) and analyzed using Student's *t*-test and nonlinear regression analysis. All experiments for cell cultures were performed independently at least three times. A *p*-value of <0.05 was considered statistically significant.

Results and discussion

EISA of PTC promotes macrophage repolarization *in vitro*

Given that the EISA of PTC can generate assemblies *in situ* on or inside cells,[22] we investigated whether the physiology of the macrophages could be influenced upon exposure to PTC. We chose human THP-1 monocytes and the murine macrophage cell line RAW264.7 for *in vitro* experiments. The suspended THP-1 monocytes incubated with PMA turned adherent and showed increased gene expression of the macrophage marker CD68 (Fig. S1A–C†). To obtain M2 macrophages, the cells were further treated with IL-4 and IL-13, showing elevated expression of M2 markers including CD206 and IL-10 (Fig. S1D†). RAW264.7 cells were treated with IL-4 directly for M2 polarization (Fig. S1E†).[31] The polarization of the macrophages was determined by measuring the levels of M2-type mRNA expressions *via* qRT-PCR. It's worth noting that very limited cytotoxicity towards the macrophages was observed after 48 h exposure to PTC even with the concentration increasing up to 10 μg mL^{-1} (Fig. S2A and B†). After 48 h exposure to 1 μg mL^{-1} PTC, M2 macrophages derived from THP-1 significantly decreased the mRNA levels of M2-related CD206 and IL-10 markers, while remarkably upregulating the M1-related TNF-α and iNOS markers (Fig. 2A). The ELISA of the supernatant from the treated macrophages further indicates a decreased production of IL-10 (Fig. 2B, $P < 0.05$), a typical M2 marker, as well as an increased secretion of TNF-α which is a typical M1 marker (Fig. 2C, $P < 0.05$). Similar results were obtained after incubating PTC with M2 macrophages derived from RAW264.7 cells (Fig. 2D–F), suggesting that the EISA of PTC can re-educate M2 macrophages towards the M1 phenotype.

We further investigated the impact of the EISA on macrophage repolarization using ascites macrophages isolated from ovarian cancer patients. The separated macrophages were treated with 5 μg mL^{-1} PTC for 48 h and then collected for flow cytometry. A group of untreated cells was used as a control. As shown in Fig. 2G and H, the ascites macrophages exhibited a lower percentage and a decreased median fluorescence intensity (MFI) of CD206 after 48 h exposure in comparison with those of the control (Fig. 2G and H). The MFI of CD86 was also increased significantly (Fig. 2I and J). The investigation of these clinical specimens further verifies the ability of the EISA to repolarize macrophages from the M2 to M1 phenotype, in good agreement with the results obtained from the

 This journal is © The Royal Society of Chemistry 2020

Published on 12 February 2020. Downloaded by Westlake University on 6/12/2025 7:47:11 AM.

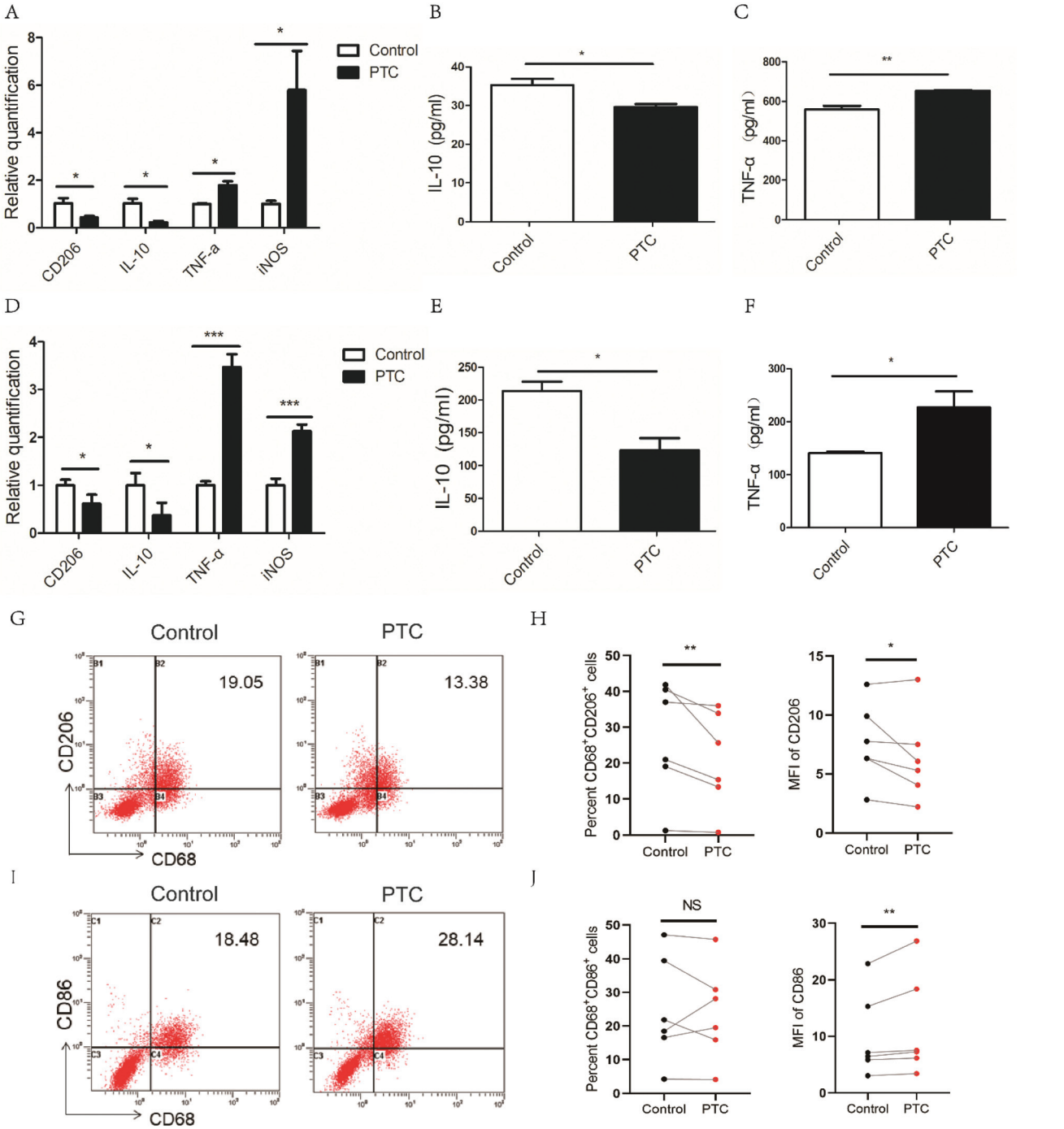

Fig. 2 Effects of PTC on TAM repolarization *in vitro*. (A) Expression of M2-related markers: CD206 and IL-10, and M1-related markers: TNF-α and iNOS were measured by qRT-PCR in THP-1-derived M2 macrophages with PTC treatment (1 μg mL^{-1}). * $P < 0.05$. (B, C) ELISA analysis of the expression of IL-10 (B) and TNF-α (C) in THP-1-derived M2 macrophages with PTC treatment (1 μg mL^{-1}). * $P < 0.05$, ** $P < 0.01$. (D) Expressions of CD206, IL-10, TNF-α and iNOS were measured by qRT-PCR in RAW264.7-derived M2 macrophages with PTC treatment (1 μg mL^{-1}). * $P < 0.05$, *** $P < 0.005$. (E, F) ELISA analysis of the expression of IL-10 (E) and TNF-α (F) in RAW264.7-derived M2 macrophages with PTC treatment (5 μg mL^{-1}). * $P < 0.05$. Error bars represent standard deviation ($n = 3$). Macrophages derived from ovarian cancer patients' ascites with PTC treatment (5 μg mL^{-1}) were separately stained with CD68-FITC, CD206-PE and CD86-APC for flow cytometric analysis. (G) Representative plots of $CD68^+CD206^+$ staining on ascites macrophage cells. (H) Quantification of the percentage of $CD68^+CD206^+$ cells and the MFI of $CD206^+$ cells. * $P < 0.05$, ** $P < 0.01$. (I) Representative plots of $CD68^+CD86^+$ staining on macrophage cells. (J) Quantification of the percentage of $CD68^+CD86^+$ cells and MFI of $CD86^+$ cells. ** $P < 0.01$. Error bars represent standard deviation ($n = 6$).

Published on 12 February 2020. Downloaded by Westlake University on 6/12/2025 7:47:11 AM.

macrophages derived from human THP-1 monocytes and murine RAW264.7 cells.

Macrophage repolarization is associated with ROS production and actin disturbance

In consideration of the critical roles of ROS for the activation and functions of M1 macrophages,[32] we then measured the levels of ROS in the macrophages after exposure to PTC. Immunofluorescence, flow cytometry and absorbance values were used to study the ROS production. According to the results of immunofluorescence (Fig. 3A and E), M2 macrophages derived from both THP-1 and RAW264.7 exhibited significantly increased intensity of red fluorescence after 48 h exposure to 5 μg mL^{-1} PTC. Flow cytometric analysis further showed the higher percentage and fluorescence intensity, indicating the elevated level of ROS generation in these macrophages that were treated with PTC (Fig. 3B, C and F, G). As expected, the absorbance values (Fig. 3D and H) were also higher than those of the control group.

As part of the cytoskeleton, actin filaments play essential roles in various cellular processes, such as cell motility, growth, and division. For macrophages, it has been identified that their polarization is dramatically associated with the changes in the cell morphology.[33,34] As reported, M2 macrophages exhibit an elongated shape compared with M1 cells, which is manipulated by actin and can promote the expression of M2 phenotypic markers.[34] To examine whether the effect of the EISA on the macrophage repolarization is associated with the rearrangement of the actin filaments, phalloidin was used to investigate the changes in the actin filaments by immunofluorescence. With the incubation of PTC, the actin filaments of macrophages derived from both THP-1 and RAW264.7 mainly exhibited short and ill-defined actin filaments, suggesting that the assemblies interact with actin and disrupt the dynamics of actin, as indicated by the red fluo-

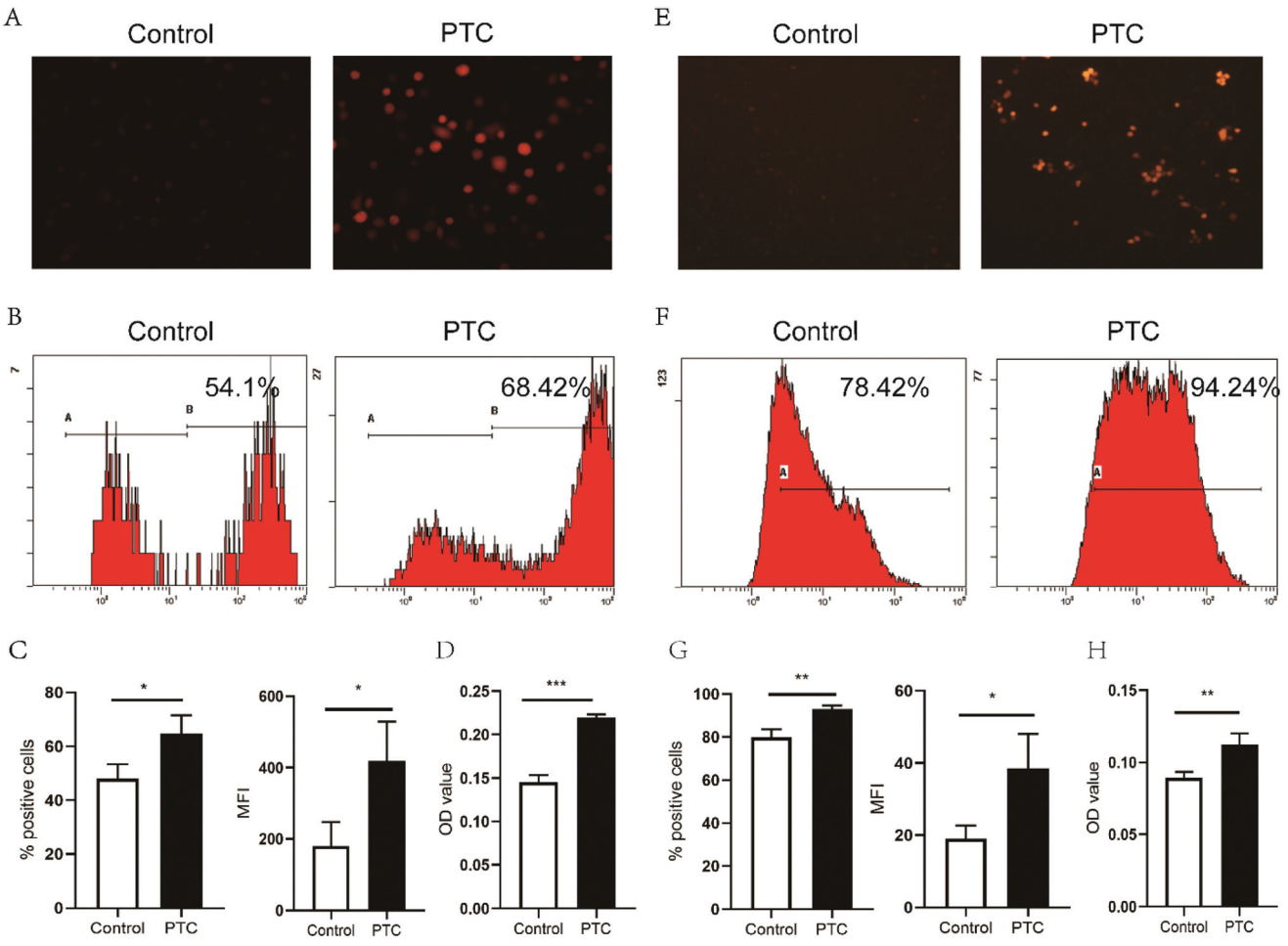

Fig. 3 ROS production of macrophages treated with PTC. (A, E) Fluorescence images showed the generation of ROS as measured using the Reactive Oxygen Species Assay Kit in THP-1-derived (A) and RAW264.7-derived (E) M2 macrophages treated with PTC (5 μg mL^{-1}). Magnification: 200×. (B, F) Flow cytometry showed the levels of ROS in THP-1-derived (B) and RAW264.7-derived (F) M2 macrophages treated with PTC (5 μg mL^{-1}). (C, G) Quantification of the percentage and MFI of positive cells in THP-1-derived (C) and RAW264.7-derived (G) M2 macrophages. (D, H) Absorbance values showed the levels of ROS at 488 mm in THP-1-derived (D) and RAW264.7-derived (H) M2 macrophages treated with PTC (5 μg mL^{-1}). * $P < 0.05$, ** $P < 0.01$, *** $P < 0.005$. Error bars represent standard deviation ($n = 3$).

This journal is © The Royal Society of Chemistry 2020

Published on 12 February 2020. Downloaded by Westlake University on 6/12/2025 7:47:11 AM.

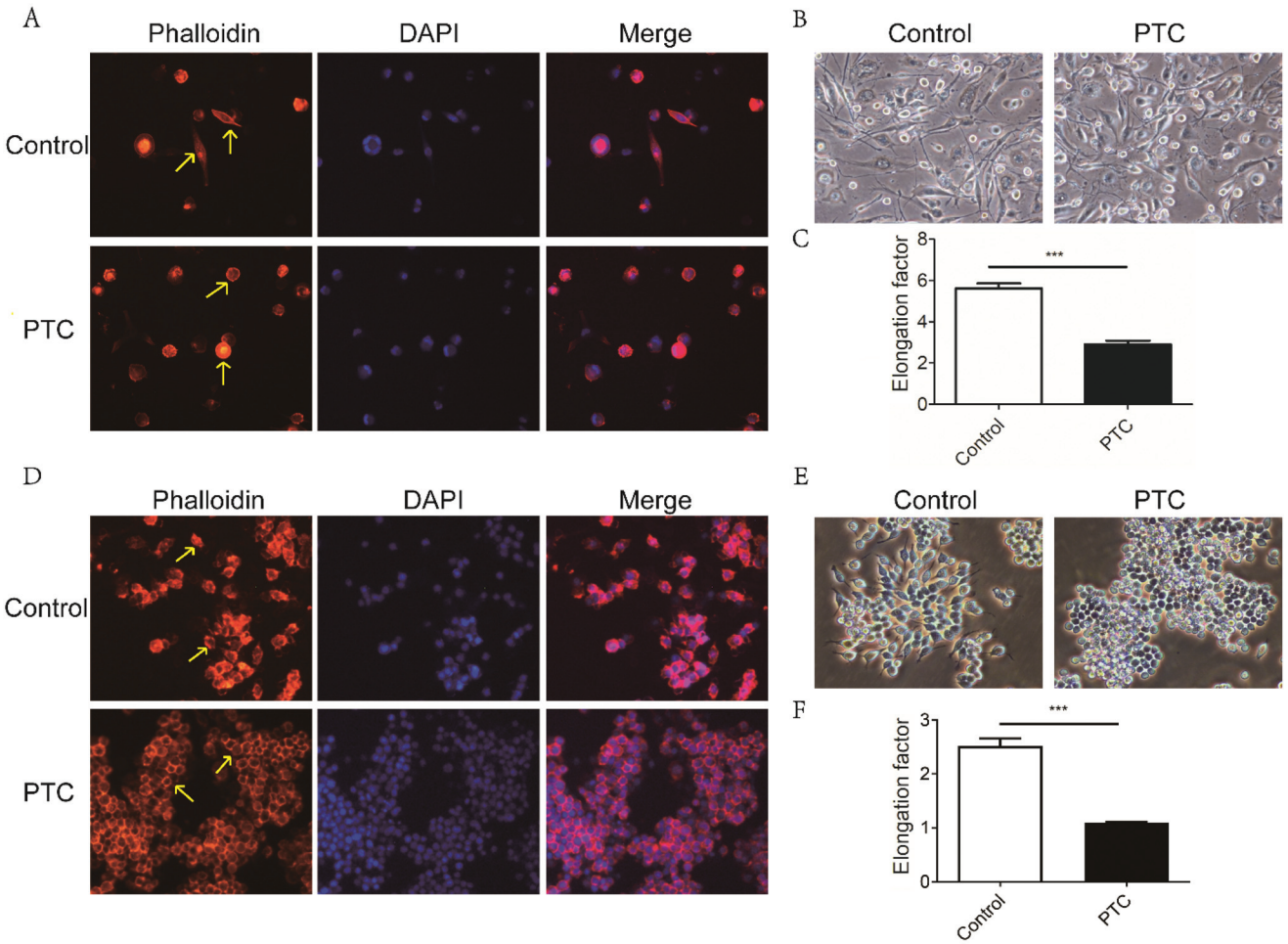

Fig. 4 Actin disturbance of macrophages treated with PTC. (A, D) Fluorescence images of THP-1-derived (A, magnification: 200×) and RAW264.7-derived (D, magnification: 400×) M2 macrophages immunostained using phalloidin (red) and DAPI (blue) with PTC treatment (5 μg mL^{-1}). Arrows highlight the difference after treatment. (B, E) Phase contrast images of THP-1-derived (B, magnification: 200×) and RAW264.7-derived (E, magnification: 400×) M2 macrophages with PTC treatment (5 μg mL^{-1}). (C, F) Quantification of the degree of THP-1-derived (C) and RAW264.7-derived (F) M2 macrophage elongation, which was defined as the length of the longest axis divided by the length of the short axis across the cell nucleus. *** $P < 0.005$. Error bars represent standard deviation ($n = 3$).

rescence shown in Fig. 4A and D. Unlike the control cells without pretreatment, the morphology of the macrophages treated with PTC varied significantly (Fig. 4B and E). The elongation of the macrophages, which is defined as the length of the longest axis divided by the length of the short axis across the cell nucleus, decreased by 50% after treatment (Fig. 4C and F). Collectively, the EISA of PTC could result in an elevated level of ROS and alteration of actin filaments in the macrophages, which in turn resulted in the repolarization from the M2 to M1 phenotype.

Dual repolarization and inhibition effects of the EISA of PTC

Having confirmed the repolarization of the macrophages, we then turned our attention to determine the direct inhibitory effect of the EISA against cancer cells. As a leading cause of death among patients diagnosed with gynecological malignancies worldwide, ovarian cancer has received increasing attention.[35] The inhibition potency of PTC against human SKOV3 and murine ID8 ovarian cancer cells was tested by using a cell counting kit-8 (CCK-8) assay. As shown in Fig. 5A and B, the half maximal inhibitory concentrations (IC_{50}) of PTC against SKOV3 and ID8 cells after 48 h incubation were calculated to be 5.48 ± 0.082 and 2.15 ± 0.075 μg mL^{-1}, respectively. Flow cytometric analysis showed that the apoptosis rate of the treated cells increased remarkably compared to the control (Fig. S3A–D†), which further demonstrates that the exposure to PTC could effectively inhibit the growth of ovarian cancer cells.

We further evaluated the dual repolarization and inhibition effects of PTC by co-incubating ovarian cancer cells with macrophages in a dual-chamber transwell plate, a simulated tumor microenvironment. M2 macrophages derived from either THP-1 or RAW264.7 were cultured on the top layer of the plate (Fig. 5C). After 48 h exposure to 5 μg mL^{-1} PTC, SKOV3 cells co-cultured with M2 macrophages derived from THP-1

Published on 12 February 2020. Downloaded by Westlake University on 6/12/2025 7:47:11 AM.

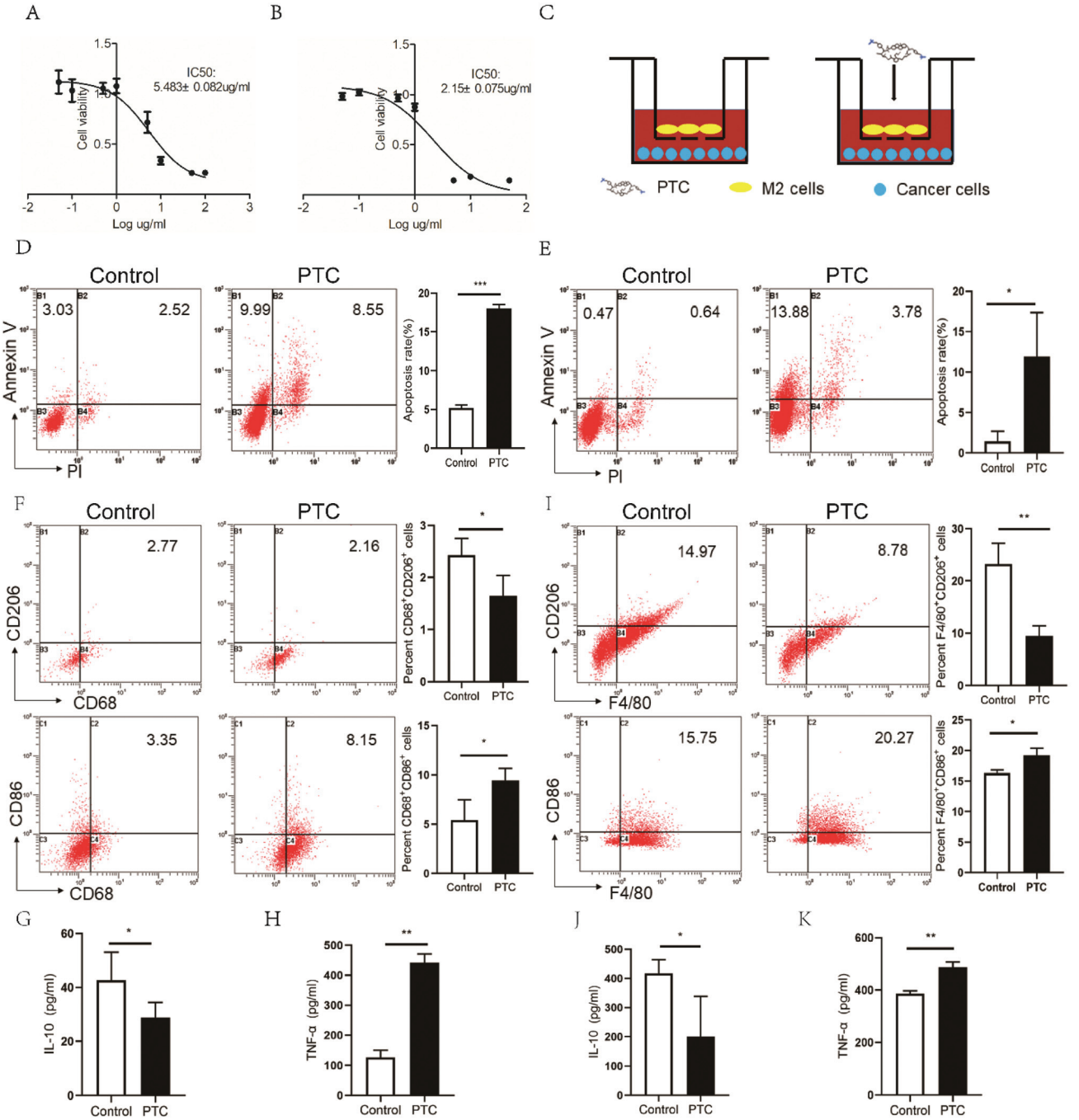

Fig. 5 Dual repolarization and inhibition effect of PTC *in vitro*. (A, B) Cytotoxicity of PTC treatment in SKOV3 (A) and ID8 (B) cells. (C) The co-culture system of the ovarian cancer cells and macrophages were established by using a transwell assay, with macrophages in the upper chamber and cancer cells in the lower chamber. The cells were separated using a 0.4 μm-sized microporous membrane, which allowed for the exchange of molecules, but not cells. (D) SKOV3 cells co-cultured with THP-1-derived M2 macrophages were stained with Annexin V and PI by flow cytometry after PTC (5 μg mL^{-1}) treatment for 48 h. Annexin V and PI plots show the populations corresponding to early (Annexin V^+PI^-) and late (Annexin V^+PI^+) apoptotic cells. Numbers in gates indicate the percentage of these populations. *** $P < 0.005$. (E) ID8 cells co-cultured with RAW264.7-derived M2 macrophages were treated with PTC (2 μg mL^{-1}) for 48 h and collected for the apoptosis assay. * $P < 0.05$. (F) THP-1-derived M2 macrophages co-cultured with SKOV3 cells were separately stained with CD68-FITC, CD206-PE and CD86-APC for flow cytometry after PTC treatment (5 μg mL^{-1}). Representative plots and quantification of both $CD68^+CD206^+$ and $CD68^+CD86^+$ staining on macrophage cells are shown. * $P < 0.05$. (G, H) ELISA analysis of the expression of IL-10 (G) and TNF-α (H) in the media of the SKOV3/THP-1-derived M2 macrophage co-culture system with PTC treatment. * $P < 0.05$, ** $P < 0.01$. (I) RAW264.7-derived M2 macrophages co-cultured with ID8 cells with PTC treatment (2 μg mL^{-1}) were separately stained with F4/80-PE, CD206-Percp-cy5.5 and CD86-PE-cy7 for flow cytometry. Representative plots and quantification of both $F4/80^+CD206^+$ and $F4/80^+CD86^+$ staining on macrophage cells are shown. * $P < 0.05$, ** $P < 0.01$. (J, K) ELISA analysis of the expression of IL-10 (J) and TNF-α (K) in the media of the ID8/RAW264.7-derived M2 co-culture system with PTC treatment. * $P < 0.05$, ** $P < 0.01$. Error bars represent standard deviation ($n = 3$).

 This journal is © The Royal Society of Chemistry 2020

Published on 12 February 2020. Downloaded by Westlake University on 6/12/2025 7:47:11 AM.

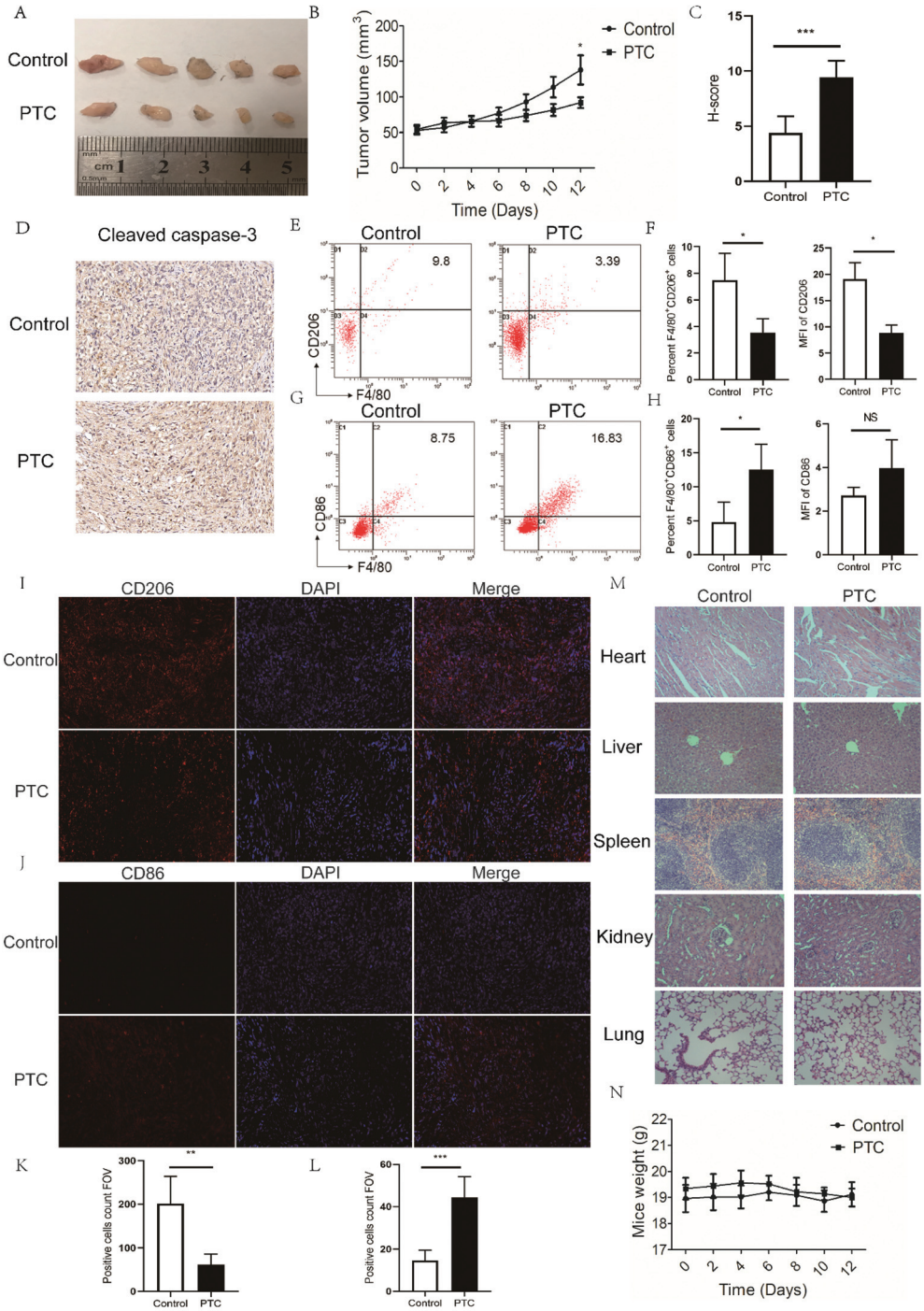

Fig. 6 Dual repolarization and inhibition effect of PTC *in vivo*. (A) Mice were randomly divided into two groups (five animals per group) and separately injected with PBS and PTC every other day. After six injections, the mice were sacrificed and the tumor tissues were harvested. (B) Tumor volume changes for tumor xenograft mice after intra-tumor injection with PBS or PTC (5 mg kg^{-1}) 6 times in total. * $P < 0.05$. (C, D) H-score (C) and representative images (D) of the IHC staining of cleaved caspase-3 in tumor tissues. *** $P < 0.005$. (E–H) Flow cytometric analysis of the cells separated from tumor tissues under PTC treatment (5 mg kg^{-1}), labeled with F4/80-PE, CD206-Percp-cy5.5 and CD86-PE-cy7. Representative plots and quantification of the percentage of $F4/80^+CD206^+$ staining and MFI of CD206 are shown in (E) and (F). Representative plots and quantification of the percentage of $F4/80^+CD86^+$ staining and MFI of CD86 are shown in (G) and (H). * $P < 0.05$. (I, J) Immunofluorescene analysis of CD206 (I) and CD86 (J) in tumor tissues after PTC treatment (5 mg kg^{-1}). Magnification: 400×. (K, L) Quantification of CD206 (K) and CD86 (L) by immunofluorescence staining. Positive cells were averaged from 5 fields of view (FOV) using a fluorescence microscope. ** $P < 0.01$, *** $P < 0.005$. (M) Pathological features of the major organs in mice treated with PBS or PTC (5 mg kg^{-1}). All tissues were stained with hematoxylin and eosin. Magnification: 200×. (N) Body weight changes for tumor xenograft mice after intra-tumor injection with PBS or PTC (5 mg kg^{-1}) 6 times. Error bars represent standard deviation ($n = 5$).

Published on 12 February 2020. Downloaded by Westlake University on 6/12/2025 7:47:11 AM.

displayed significantly increased apoptotic rates including both early and late apoptosis compared with the control group (Fig. 5D). Meanwhile, THP-1-derived macrophages co-cultured with SKOV3 cells exhibited a lower percentage of $CD68^+CD206^+$ cells and a higher percentage of $CD68^+CD86^+$ cells (Fig. 5F) as well as a decreased production of IL-10 and an increased secretion of TNF-α (Fig. 5G and H). Similar results were observed when ID8 cells were co-cultured with M2 macrophages derived from RAW264.7 (Fig. 5E and I–K), verifying the dual repolarization and inhibition effects of PTC.

Finally, we assessed the dual repolarization and inhibition effects of PTC *in vivo* using an immunocompetent murine model of ID8 ovarian cancer. Mice were intratumorally injected with PTC every other day for total 12 days. A group of mice injected with PBS was used as a control. Encouragingly, significantly suppressed tumor growth was observed after 6 injections of 5 mg kg^{-1} of PTC (Fig. 6A and B), accompanied by an increasing expression of cleaved caspase-3 after treatment (Fig. 6C and D). Flow cytometric analysis of macrophages isolated from the tumor tissues showed almost 3-times lower $CD206^+$ cells and 2-fold higher $CD86^+$ cells in comparison with those of the control (Fig. 6E–H). Immunofluorescene analysis of the tumor tissues that were sectioned from the treated mice also showed a decreased percentage of $CD206^+$ cells (Fig. 6I and K) and an increased number of $CD86^+$ cells (Fig. 6J and L), as evidenced by the intensity of red fluorescence. These results suggested the capability of EISA to repolarize macrophages *in vivo*. The biocompatibility of the EISA of PTC was also investigated. We evaluated the *in vivo* toxicity of PTC against the major organs in mice by histological analysis. After 6 doses, the tissues were immediately harvested, fixed with formalin and further embedded with paraffin. The resultant tissues were then sectioned and stained with H&E for microscopy imaging. As shown in Fig. 6M, no significant difference was observed between the tissues sectioned from mice treated with PTC and the control from mice injected with PBS (Fig. 6M). With respect to mouse body weights, no distinct difference was found between the control group and mice treated with PTC (Fig. 6N). These data imply the dual repolarization and inhibition effects of the EISA of PTC with low toxicity *in vivo*.

Conclusions

In summary, we report the use of EISA, an effective yet simple strategy, to combine tumor microenvironment immunomodulation and chemotherapy for cancer treatment. The EISA of a cholesterol based conjugate results in the assembly of its derivative in the cell milieu, which simultaneously promotes pro-inflammatory macrophage polarization and induces direct death of cancer cells. The generation of reactive oxygen species and actin disturbance induced by the assemblies has been demonstrated relative to macrophage repolarization. We also demonstrate the dual repolarization and inhibition effects *in vivo* by showing an increased number of pro-inflammatory M1 macrophages in tumor tissues and significantly inhibited tumor growth in an immunocompetent murine model of ovarian cancer. We anticipate that the use of EISA to treat various tumors by regulating multiple biological targets is a unique approach for combination cancer therapy.

Conflicts of interest

The authors have declared that no competing interest exists.

Acknowledgements

This work was financially supported by the National Key R&D Program of China (2016YFC1302900), the National Natural Science Foundation of China (81772770, 81802582, 21875135), the Program of Shanghai Hospital Development Center (16CR2001A), the Science and Technology Commission of Shanghai Municipality (18441904800), the Shanghai Municipal Commission of Health and Family Planning (2017ZZ02016), the Youth Thousand-Talents Program of China (D1410022) and the Doctor Innovation fund of Shanghai Jiao Tong University School of Medicine (BXJ201920).

Notes and references

1 Y. Wolf and Y. Samuels, *ESMO Open*, 2018, **3**, e000475.
2 H. Sun, Y. Dong, J. Feijen and Z. Zhong, *J. Controlled Release*, 2018, **290**, 11–27.
3 K. Newick, S. O'Brien, E. Moon and S. M. Albelda, *Annu. Rev. Med.*, 2017, **68**, 139–152.
4 S. C. Wei, C. R. Duffy and J. P. Allison, *Cancer Discovery*, 2018, **8**, 1069–1086.
5 L. M. Colli, M. J. Machiela, H. Zhang, T. A. Myers, L. Jessop, O. Delattre, K. Yu and S. J. Chanock, *Cancer Res.*, 2017, **77**, 3666–3671.
6 P. Sharma and J. P. Allison, *Cell*, 2015, **161**, 205–214.
7 F. J. Esteva, V. M. Hubbard-Lucey, J. Tang and L. Pusztai, *Lancet Oncol.*, 2019, **20**, e175–e186.
8 S. A. Patel and A. J. Minn, *Immunity*, 2018, **48**, 417–433.
9 A. L. Correia and M. J. Bissell, *Drug Resist. Updates*, 2012, **15**, 39–49.
10 E. S. Nakasone, H. A. Askautrud, T. Kees, J. H. Park, V. Plaks, A. J. Ewald, M. Fein, M. G. Rasch, Y. X. Tan, J. Qiu, J. Park, P. Sinha, M. J. Bissell, E. Frengen, Z. Werb and M. Egeblad, *Cancer Cell*, 2012, **21**, 488–503.
11 J. Wang, J. S. Lee, D. Kim and L. Zhu, *ACS Appl. Mater. Interfaces*, 2017, **9**, 39971–39984.
12 J. Larkin, V. Chiarion-Sileni, R. Gonzalez, J. J. Grob, C. L. Cowey, C. D. Lao, D. Schadendorf, R. Dummer, M. Smylie, P. Rutkowski, P. F. Ferrucci, A. Hill, J. Wagstaff, M. S. Carlino, J. B. Haanen, M. Maio, I. Marquez-Rodas, G. A. McArthur, P. A. Ascierto, G. V. Long, M. K. Callahan, M. A. Postow, K. Grossmann, M. Sznol, B. Dreno, L. Bastholt, A. Yang, L. M. Rollin, C. Horak, F. S. Hodi and J. D. Wolchok, *N. Engl. J. Med.*, 2015, **373**, 23–34.

 This journal is © The Royal Society of Chemistry 2020

Published on 12 February 2020. Downloaded by Westlake University on 6/12/2025 7:47:11 AM.

13 J. Zhou and B. Xu, *Bioconjugate Chem.*, 2015, **26**, 987–999.
14 Y. Gao, J. Shi, D. Yuan and B. Xu, *Nat. Commun.*, 2012, **3**, 1033.
15 Q. Yao, Z. Huang, D. Liu, J. Chen and Y. Gao, *Adv. Mater.*, 2019, **31**, e1804814.
16 J. Li, Y. Kuang, J. Shi, J. Zhou, J. E. Medina, R. Zhou, D. Yuan, C. Yang, H. Wang, Z. Yang, J. Liu, D. M. Dinulescu and B. Xu, *Angew. Chem., Int. Ed.*, 2015, **54**, 13307–13311.
17 J. Zhou, X. Du, N. Yamagata and B. Xu, *J. Am. Chem. Soc.*, 2016, **138**, 3813–3823.
18 F. Zhao, B. A. Heesters, I. Chiu, Y. Gao, J. Shi, N. Zhou, M. C. Carroll and B. Xu, *Org. Biomol. Chem.*, 2014, **12**, 6816–6819.
19 Y. Gao, C. Zhang, J. Chang, C. Yang, J. Liu, S. Fan and C. Ren, *Biomater. Sci.*, 2019, **7**, 1477–1485.
20 A. Tanaka, Y. Fukuoka, Y. Morimoto, T. Honjo, D. Koda, M. Goto and T. Maruyama, *J. Am. Chem. Soc.*, 2015, **137**, 770–775.
21 L. Dong, J. Qian, Z. Hai, J. Xu, W. Du, K. Zhong and G. Liang, *Anal. Chem.*, 2017, **89**, 6922–6925.
22 H. Wang, Z. Feng, D. Wu, K. J. Fritzsching, M. Rigney, J. Zhou, Y. Jiang, K. Schmidt-Rohr and B. Xu, *J. Am. Chem. Soc.*, 2016, **138**, 10758–10761.
23 H. Wang, Z. Feng, C. Yang, J. Liu, J. E. Medina, S. A. Aghvami, D. M. Dinulescu, J. Liu, S. Fraden and B. Xu, *Mol. Cancer Res.*, 2019, **17**, 907–917.
24 W. Yang, Y. Bai, Y. Xiong, J. Zhang, S. Chen, X. Zheng, X. Meng, L. Li, J. Wang, C. Xu, C. Yan, L. Wang, C. C. Chang, T. Y. Chang, T. Zhang, P. Zhou, B. L. Song, W. Liu, S. C. Sun, X. Liu, B. L. Li and C. Xu, *Nature*, 2016, **531**, 651–655.
25 F. Wang, K. Beck-Garcia, C. Zorzin, W. W. Schamel and M. M. Davis, *Nat. Immunol.*, 2016, **17**, 844–850.
26 Y. Singh, V. K. Pawar, J. G. Meher, K. Raval, A. Kumar, R. Shrivastava, S. Bhadauria and M. K. Chourasia, *J. Controlled Release*, 2017, **254**, 92–106.
27 Y. Wang, Y. X. Lin, S. L. Qiao, H. W. An, Y. Ma, Z. Y. Qiao, R. P. Rajapaksha and H. Wang, *Biomaterials*, 2017, **112**, 153–163.
28 R. Noy and J. W. Pollard, *Immunity*, 2014, **41**, 49–61.
29 P. Pathria, T. L. Louis and J. A. Varner, *Trends Immunol.*, 2019, **40**, 310–327.
30 S. Zanganeh, G. Hutter, R. Spitler, O. Lenkov, M. Mahmoudi, A. Shaw, J. S. Pajarinen, H. Nejadnik, S. Goodman, M. Moseley, L. M. Coussens and H. E. Daldrup-Link, *Nat. Nanotechnol.*, 2016, **11**, 986–994.
31 M. Song, T. Liu, C. Shi, X. Zhang and X. Chen, *ACS Nano*, 2016, **10**, 633–647.
32 A. Sindrilaru, T. Peters, S. Wieschalka, C. Baican, A. Baican, H. Peter, A. Hainzl, S. Schatz, Y. Qi, A. Schlecht, J. M. Weiss, M. Wlaschek, C. Sunderkotter and K. Scharffetter-Kochanek, *J. Clin. Invest.*, 2011, **121**, 985–997.
33 C. B. Rodell, S. P. Arlauckas, M. F. Cuccarese, C. S. Garris, R. Li, M. S. Ahmed, R. H. Kohler, M. J. Pittet and R. Weissleder, *Nat. Biomed. Eng.*, 2018, **2**, 578–588.
34 F. Y. McWhorter, T. Wang, P. Nguyen, T. Chung and W. F. Liu, *Proc. Natl. Acad. Sci. U. S. A.*, 2013, **110**, 17253–17258.
35 R. L. Siegel, K. D. Miller and A. Jemal, *CA-Cancer J. Clin.*, 2018, **68**, 7–30.